applied sciences

MDPI

Article

Investigations on Pressure Broadening Coefficients of NO Lines in the 1←0 Band for N_2, CO_2, Ar, H_2, O_2 and He

Sumit Agarwal [1,*], Leopold Seifert [1], Denghao Zhu [1], Bo Shu [1], Ravi Fernandes [1,2] and Zhechao Qu [1,*]

[1] Department of Physical Chemistry, Physikalisch-Technische Bundesanstalt, 38116 Braunschweig, Germany
[2] Institute of Internal Combustion Engines, Technische Universität Braunschweig, 38106 Braunschweig, Germany
* Correspondence: sumit.agarwal@ptb.de (S.A.); zhechao.qu@ptb.de (Z.Q.); Tel.: +49-5315923112 (ext. 3386) (S.A.); +49-5315923112 (ext. 3112) (Z.Q.)

Abstract: A tunable diode laser absorption spectroscopy (TDLAS)-based spectrometer employing a mid-infrared (Mid-IR) interband cascade laser (ICL) was developed and used to determine pressure broadening coefficients of two NO absorption transitions at 1914.98 cm^{-1} and 1915.76 cm^{-1} in the fundamental (1←0) band (R11.5 Ω1/2 and Ω3/2) for CO_2, N_2, Ar, O_2, He, and H_2. For the first time, a reliable and consistent set of six different pressure-broadening coefficients for the NO line has been measured by a consistent approach covering pressures from 100 to 970 mbar at a temperature of 294 K. Air pressure broadening has been calculated based on N_2 and O_2 coefficients. The stated pressure-broadening coefficients for N_2, CO_2, Ar, H_2, O_2, He, and Air have relative errors in the 0.5–1.5% range. For CO_2 and H_2, broadening results of NO (1←0) band (R11.5 Ω1/2 and Ω3/2) lines are reported for the first time. The results are also compared to previously available literature data. It was found that the broadening coefficients for O_2 and Air are in agreement with literature values, whereas results for Ar and He show larger differences.

Keywords: absorption spectroscopy; broadening coefficient; Nitric Oxide; uncertainty

check for updates

Citation: Agarwal, S.; Seifert, L.; Zhu, D.; Shu, B.; Fernandes, R.; Qu, Z. Investigations on Pressure Broadening Coefficients of NO Lines in the 1←0 Band for N_2, CO_2, Ar, H_2, O_2 and He. *Appl. Sci.* **2023**, *13*, 1370. https://doi.org/10.3390/app13031370

Academic Editor: Alessandra Biancolillo

Received: 22 December 2022
Revised: 16 January 2023
Accepted: 18 January 2023
Published: 20 January 2023

Copyright: © 2023 by the authors. Licensee MDPI, Basel, Switzerland. This article is an open access article distributed under the terms and conditions of the Creative Commons Attribution (CC BY) license (https://creativecommons.org/licenses/by/4.0/).

1. Introduction

Nitric oxide (NO) is a major polluting chemical species in the atmosphere and has a special role in the destruction of the stratospheric ozone layers, as sunlight helps NO to react with the Ozone to form oxygen [1–4]. NO can be produced from different sources, such as natural, biogenic and industrial processes [5–7].

When coming from natural sources, NO is mainly produced inside thunderstorms. In the case of biogenic origin, it can be produced from agricultural fertilization. Moreover, three pathways of NO formation from industrial sources exist, namely, thermal NO, fuel NO and prompt NO. In the case of thermal NO, the major source is the high-temperature combustion of, say, natural gas in the air. The major contribution of NO comes from transportation fuel. Regarding the formation of prompt NO, it occurs mainly in low-temperature oxidation of hydrocarbons under rich conditions, which are prominent in non-premixed combustion, such as in diesel engines [8,9].

NO is an essential component when it comes to air pollution caused by thermal power plants, combustion engines (e.g., vehicle emission) and aero engines [6,7]. The effect of NO formation in heated air or in the exhaust gases produced by the oxidative reaction of nitrogen has been well elaborated [8]. The effect of high-temperature NO formation can be significantly seen in the form of photochemical smog. The NO, in turn, combines with water vapor in the air to form nitric acid, which is one component of acid rain. As is known from the eminent Zeldovich equations [8,9] regarding temperature, the formation of NO above 1593 K is limited by the availability of the oxygen content in the air, while in temperatures below 1033 K, there is either no formation of NO or an extremely low concentration. NO is largely generated by human activity, where combustion-based mobility contributes about half of the total NO emissions. The accurate quantification of NO is of paramount interest.

Sensitive, selective and online laser-based trace gas detection is an effective method for non-invasive diagnostics [10,11]. NO sensors based on tunable laser absorption spectroscopy (TDLAS) have been proven to be a suitable candidate to monitor NO levels because of their capability to provide sensitive, accurate, in situ and absolute measurements for various conditions, even in harsh environments [12]. Accurate spectral line parameters of the targeted molecule (such as pressure broadening coefficient and line strength) are critical for TDLAS spectrometers in the context of a precise amount of fraction monitoring of trace species with a low signal-to-noise ratio [13–15].

For example, fixed wavelength TDLAS has been normally used in shock tube experiments, and the spectral line parameters (pressure broadening or cross-section) are essential for species quantification. The pressure-broadening coefficient of NO has been investigated by many researchers, including both theoretical and experimental aspects [16–20]. In 1982, Lundqvist attempted to measure the pressure-broadening coefficient for R-branch lines of NO near 5.4 μm using a computerized tunable diode laser spectrometer [17]. Further, Vyrodov et al. measured the lineshape parameters of NO $A \rightarrow X(0,0)$ transitions broadened by Ar, He and N_2 using Laser Induced Fluorescence (LIF) at room temperature [21]. In another study, Chang et al. utilized a rapid tuning intracavity-doubled continuous-wave (CW) dye laser to resolve absorption lineshapes in the NO $A \leftarrow X\ (0,0)$ band at 226 nm and obtain the room-temperature broadening coefficient for argon as 0.503 cm^{-1} atm^{-1} and for nitrogen as 0.583 cm^{-1} atm^{-1}, respectively [22]. So, an accurate and consistent spectroscopic database is needed for quantitative species measurements. For the exact quantification of NO, it is important to carefully measure the spectral line parameters [11,22]. The current study focuses on the measurement of NO (R11.5) Ω3/2 and Ω1/2 transition lines in the 1-0 band. Six pressure broadening coefficients for NO—CO_2, -O_2, -N_2, -He, -H_2 and -Ar—are obtained based on the same experimental set-up and the data evaluation methodology.

2. Methodology

We have used the well-known TDLAS approach to precisely quantify the pressure-broadening coefficient of the NO transition line in the mid infrared (Mid-IR) band. For the TDLAS, the transmitted intensity through a gaseous sample can be estimated using the renowned Beer–Lambert's law [23,24]:

$$I(\nu) = E(t) + I_0(\nu) \cdot T(t) \cdot exp[-S(T) \cdot g(\nu - \nu_0) \cdot n \cdot L] \quad (1)$$

with $E(t)$ being the background emission at time t, $I_0(\nu)$ being the initial laser intensity, and $T(t)$ representing the losses due to broadband transmission, which is simultaneously derived from the individual raw signals and absorption profiles, respectively. The absorption line strength at gas temperature T is represented by the term in the exponential term, which is $S(T)$; $g(\nu - \nu_0)$ is the normalized (integrated area = 1) line shape function with a centered wavenumber of ν_0, n is the absorber number density, and L is the optical path length. Finally, one can compute the absorbance spectrum from the following equation as stated:

$$\alpha = -\ln\left(\frac{I(\nu) - E(t)}{I_0(\nu) \cdot T(t)}\right) = S(T) \cdot g(\nu - \upsilon_0) \cdot n \cdot L \quad (2)$$

To model the absorbance spectrum's lineshape in Equation (2), the Voigt function was taken, as it considers the combined effects on the spectral line caused due to Doppler and collisional broadening. Its effect is distinguished by the Doppler broadening full width at half maximum (FWHM), $\Delta\nu_D$ and the collisional-broadening FWHM, $\Delta\nu_L$, given by

$$\Delta\upsilon_D = \upsilon_0 \sqrt{\frac{8k_B T \ln 2}{Mc^2}} \quad (3)$$

$$\Delta\upsilon_L = 2 \cdot p \cdot \gamma_{self} \cdot x + 2 \cdot p \cdot \gamma_f \cdot (1 - x) \quad (4)$$

in which x represents the NO amount fraction, k_B is the Boltzmann constant, M is the molecular mass of the absorbing species, c is the speed of light, p is the total pressure, and the coefficients γ_{self} and γ_f are the self and foreign broadening coefficients that depend on the gas temperature T, respectively. Since the gas temperature is measured in the experiment, the Doppler broadening coefficient can be determined using Equation (3). It is also important to keep in mind that the broadening coefficients (γ_{self}, γ_f) determined by applying Equation (4) are the corresponding values at an experimental temperature, T, and have not been modified to the reference temperature T_0 = 296 K, which is utilized in HITRAN [25]. The broadening coefficients must be converted to a specific temperature using the self- and foreign-temperature dependency coefficients (n_{self} and n_f). Typically, n_{self} and n_f often have values between 0.4 and 0.9 [25].

3. Technical Details of the Experiments

Figure 1 depicts the experimental setup for determining the NO pressure broadening coefficients, which is similar to the setup used in other studies [23,26]. To measure the transition lines in the NO 1←0 fundamental band, a 5.2 µm interband cascade laser (ICL) (Nanoplus GmbH) was used. To capture the targeted transition lines using the wavelength scanned TDLAS technique, the NO laser current was scanned by a 140 Hz linear saw-tooth-shaped signal generated by a function generator (Agilent, 33220B). A low-noise laser current driver (Thorlabs, LDC8002) controls the laser current, while a Peltier-element controlled by a temperature controller stabilizes the laser temperature (Thorlabs TEC8020). In this study, a 7 cm long stainless-steel single-pass gas cell with two CaF2 windows was used. The laser beam was focused onto a photodetector after passing through the gas cell (VIGO, PVI-4TE-5). A 16-bit 625 kSps DAQ card was used to record the detector output signal (National Instruments, PXI-6363). An absolute capacitance manometer (AA02A Baratron by MKS, range 1000 mbar) was used to measure gas pressure. A Pt100 sensor was used to measure the temperature of the gas cell. Both temperature and pressure sensors were calibrated and are traceable to the SI using PTB's national pressure and temperature standards.

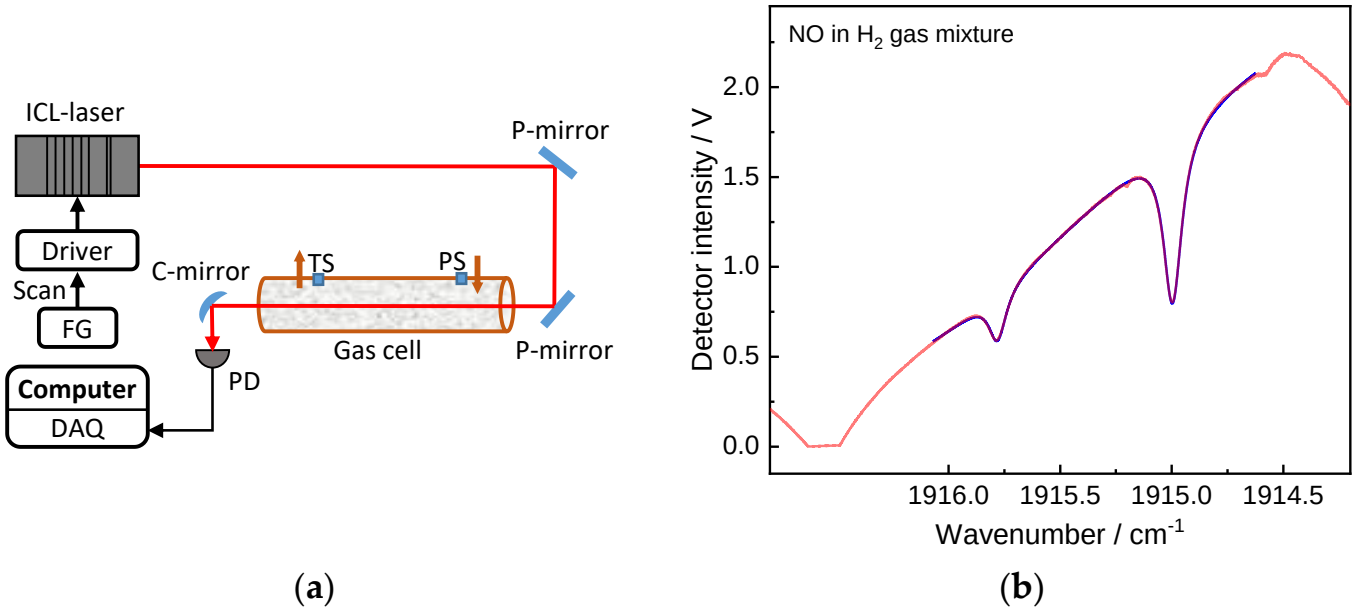


Figure 1. (**a**) The spectrometer's experimental configuration for determining the pressure broadening coefficients, where PS: pressure sensor; PD: photodetector; FG: function generator; DAQ: data acquisition card; (**b**) Measured typical laser intensity with two NO absorption peaks.

The optical set-up is depicted in detail in Figure 1a, showing the alignment of the laser beam. The absorbing beam shown in red was coupled into the gas cell via two mirrors and projected onto the detector surface by another concave mirror. Before each experiment, a

Germanium crystal etalon (Q-MACS, Length 76.25 mm) was placed in the beam path to generate the interference signal that was used to calculate the optical frequency domain of the scanned frequency range (i.e., to convert the *x*-axis domain to wavenumber).

4. Results and Discussion

High-quality pure NO and buffer gas cylinders (purity 5.0, Linde, Dublin, Ireland) were used in the experiments of measuring the foreign broadening coefficients. The manometric gas mixtures were configured via partial pressure that follows Dalton's law. The gas mixture preparation procedure is as follows: (1) evacuate the whole system (<10^{-3} mbar), including the gas cell and all components in the gas manifold up to the gas cylinder; (2) flush the gas cell with pure NO and then evacuate the system; (3) repeat step 2 for 3 times; (4) filling pure NO into the gas cell with the pressure less than 0.5 mbar; (5) fill the buffer gas (e.g., Ar, O_2, N_2, H_2, He and CO_2) to the pre-defined value. The exhaust pump and gas cell outlet valve both control the cell's gas pressure. The resulting cell pressure was lying in the range of 100 to 1000 mbar. The measured temperature stayed at 294 K throughout the measurement campaign. In Figure 1b, there are two NO absorption peaks within the spectral window. The line list from HITRAN is shown in Table 1 [25]. To perform the lineshape fitting for the measured spectrum, 10 NO lines in each absorption peak are fitted using the Voigt profile. Within Peak 1 ($\Omega 1/2$) or Peak 2 ($\Omega 3/2$) transition lines, the 10 NO lines have the same broadening coefficient, temperature dependence and lower state energy. The transition lines as shown in Table 1 are valid for the newly identified broadening coefficients in this study.

Table 1. The HITRAN database's line list.

Peak	Wavenumber (cm^{-1})	Line Strength (cm^{-2} atm^{-1})	Line Number
Peak 1 $\Omega 1/2$	1914.984827	1.474×10^{-20}	R11.5e
	1914.984833	1.597×10^{-20}	R11.5e
	1914.984854	1.731×10^{-20}	R11.5e
	1914.986297	1.029×10^{-22}	R11.5e
	1914.986307	1.029×10^{-22}	R11.5e
	1914.992367	1.028×10^{-22}	R11.5f
	1914.992494	1.028×10^{-22}	R11.5f
	1914.994619	1.730×10^{-20}	R11.5f
	1914.994622	1.473×10^{-20}	R11.5f
Peak 2 $\Omega 3/2$	1915.767290	9.245×10^{-21}	R11.5e
	1915.767318	5.494×10^{-23}	R11.5e
	1915.767321	5.494×10^{-23}	R11.5e
	1915.767342	8.530×10^{-21}	R11.5e
	1915.767384	7.869×10^{-21}	R11.5e
	1915.769033	5.494×10^{-23}	R11.5f
	1915.769214	9.244×10^{-21}	R11.5f
	1915.769217	5.494×10^{-23}	R11.5f
	1915.769246	8.529×10^{-21}	R11.5f

4.1. CO_2 Broadening Coefficient

A NO/CO_2 gas mixture was prepared using the above-mentioned gas mixture preparation procedure to derive the NO-CO_2 broadening coefficient. Figure 2a depicts a subset of the measured NO/CO_2 gas mixture line profiles at two pressures. The measured lines were averaged across 20 scans, and the Voigt model was fitted with a third-order background polynomial and a non-linear Levenberg–Marquart technique. Two absorption peaks were fitted simultaneously as well as a CO_2 line between two NO peaks.

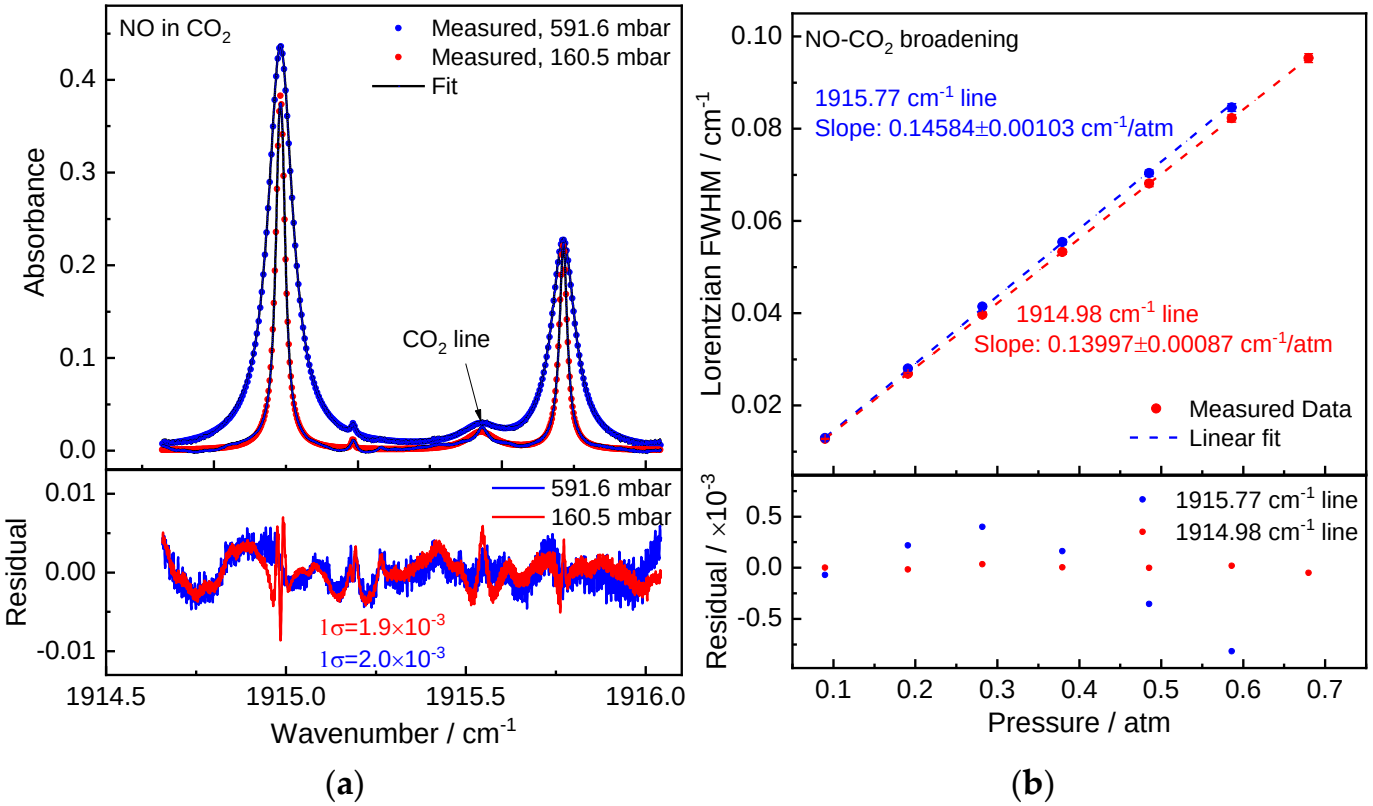


Figure 2. (**a**) Measured NO absorption spectra (averaged over 20 scans) in CO_2 at pressures of 160.5 mbar and 591.6 mbar. Below is a display of the residual between the measured and fitted values. (**b**) A linear fitted model utilized to measured CO_2-induced pressure broadening of two NO absorption peaks. Shown below are the residual between fit and data.

The spectra fitting residuals were around (1σ) 2×10^{-3} optical density, as shown in Figure 2a. The signal-to-noise-ratio (SNR) was close to 200 when compared to the absorption peak. In our spectra fitting algorithm, the Gaussian width was calculated according to Equation (3) using the gas temperature measured by the temperature sensor. The Lorentzian line width was set as a fitting parameter. A linear regression was used to calculate the pressure broadening coefficient γ_f from the fitted Lorentzian line widths at different pressures. According to the calibration certificate from PTB, the uncertainty (k = 1) of the pressure values was in the range of 0.1–0.15 mbar. As shown in Figure 2b, the pressure uncertainty was used as the x-error bar in the linear regression. The 1 standard deviation of the Lorentzian line width results (multiple measurements, typical 50–100 spectra) at each pressure step was used as the y-error bar, along with the uncertainty of the relative laser wavelength. As described in Equation (4), the fitted Lorentzian line widths exhibit very good linearity with pressures (only the second term, as the self-broadening contribution is negligible due to the trace NO level in the gas cell). Thus, we determined NO-CO_2 broadening coefficients of γ_{co2} = 72.92(52) $\times$ 10^{-3} cm^{-1}/atm and 79.99(44) $\times$ 10^{-3} cm^{-1}/atm for Peak 1 and 2, respectively.

4.2. N_2 Broadening Coefficient

NO/N_2 gas mixtures were prepared in the gas cell in the same manner as the NO/CO_2 experiment to determine the N_2 broadening coefficient. Figure 3a depicts a measured absorption spectrum at pressures of 896.1 mbar and 198.6 mbar, respectively. The residuals of the fitting were in the neighborhood of (1σ) 5×10^{-3} optical density. With pressures falling within the measurement pressure range, the measured Lorentzian widths exhibit very good linearity. The measured NO-N_2 broadening coefficients are γ_{N2} = 58.13(31) $\times$ 10^{-3} cm^{-1}/atm and 50.80(27) $\times$ 10^{-3} cm^{-1}/atm for Peak 1 and 2.

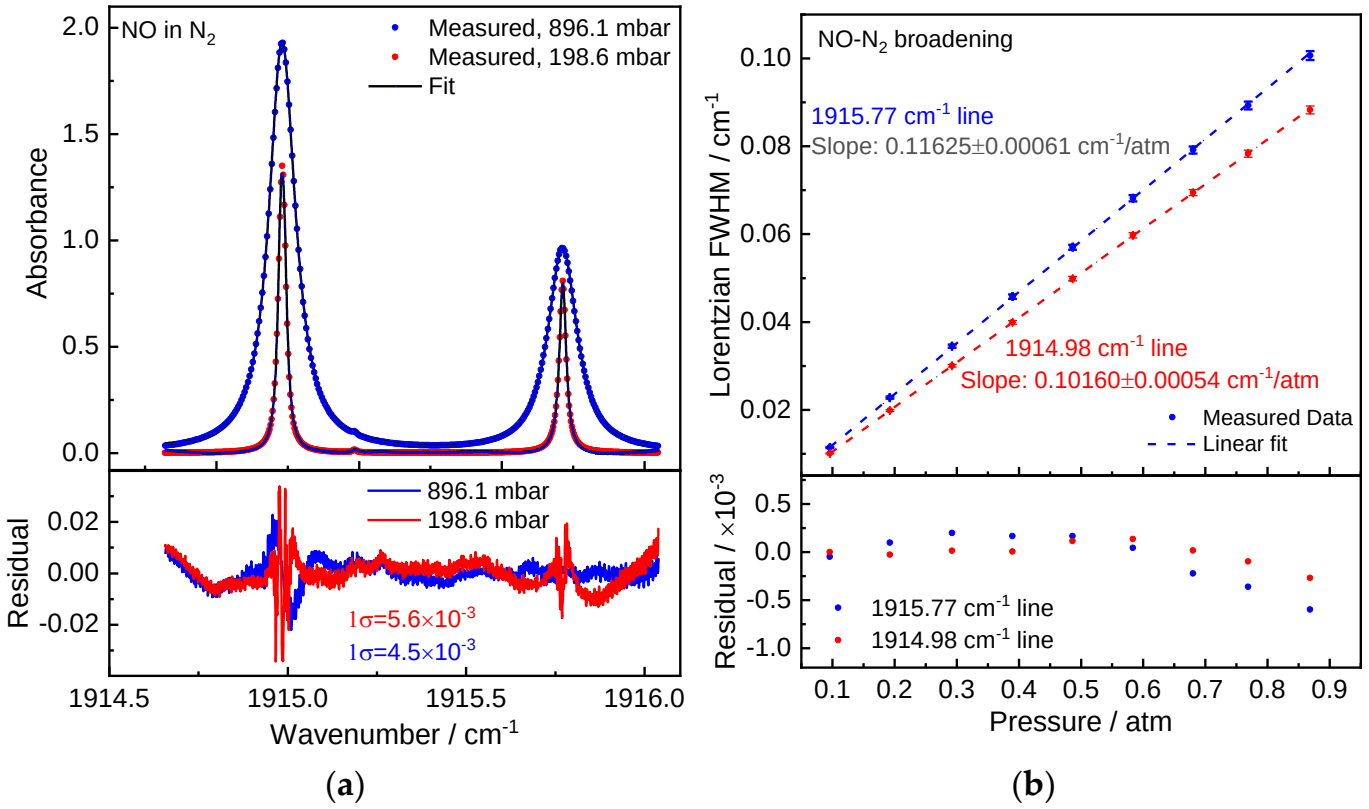


Figure 3. (**a**) Measured NO absorption spectra in N2 at pressures of 896.1 mbar and 198.6 mbar (20-scan averaged). The residual between the measured and fitted data is depicted below, yielding an SNR of ~300. (**b**) Experimentally obtained N_2-induced pressure broadening of the NO absorption lines with a linear fitting model. The residual between fit and data is depicted in the graph below.

4.3. Broadening Coefficient, Ar

The same method was used to conduct the measurements of NO-Ar broadening. The spectrum treatment was the same as for measurements of CO_2 and N_2 broadening. Figure 4a shows the measured NO absorption spectrum in Ar (938.3 mbar and 143.4 mbar, 294 K), the fitting residuals were around (1σ) 3–4 × 10^{-3} (optical density). Figure 4 displays the measured Lorentzian widths at various pressures (b). For Peaks 1 and 2, respectively, the measured NO-Ar broadening coefficients from the linear fit slopes are γ_{Ar} = 42.64(22) × 10^{-3} and 37.67(19) × 10^{-3} cm^{-1}/atm. Additionally, the NO concentration measurement in the gas-phase oxidation of ammonia under 90% argon dilution determined in the temperature range of 1581–2720 K near 3 bar is being used and well validated with the evaluated Ar broadening coefficient data. More details on the measurement are available in the reference [27].

4.4. Broadening Coefficient, O_2

The measuring process for NO-O_2 broadening was the same as for the other studies. Pure O2 was employed as the buffer gas here (purity 5.0, Linde). NO will react with O_2 to form NO_2 during the experiment as well as the gas mixture preparation process. NO concentration deduction was observed when filling O_2 into the gas cell. The maximum pressure used in NO-O_2 broadening measurement was less than 400 mbar. As an example, Figure 5a depicts an absorption spectrum of NO in O_2 measured at total pressures of 144.1 mbar and 295.9 mbar. The observed spectrum was averaged over 20 scans, and the Voigt profile was used to fit it. The obtained NO-O_2 broadening coefficient is γ_{O2} = 57.68(66) × 10^{-3} cm^{-1}/atm and 50.88(53) × 10^{-3} cm^{-1}/atm for Peak 1 and Peak 2 according to the slopes of the linear regression of the Lorentzian widths versus pressures.

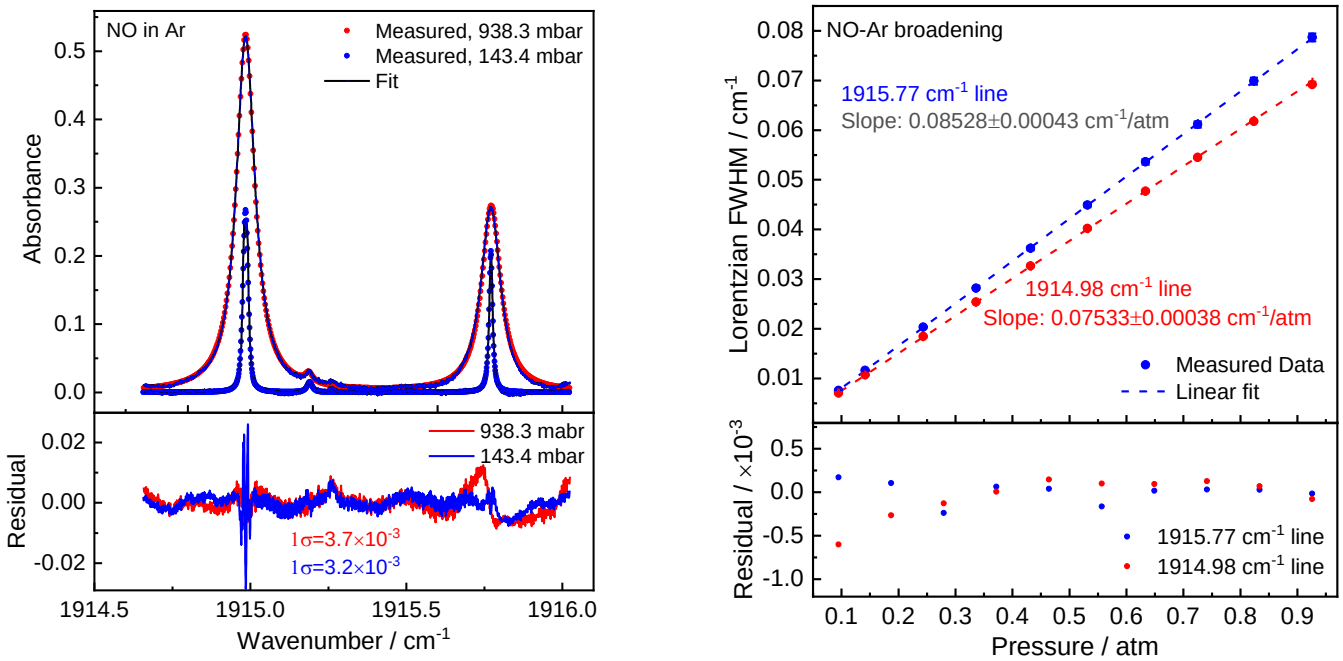


Figure 4. (**a**) Measured NO absorption spectra (20-scan averaged) in Ar at pressures 938.3 mbar and 143.4 mbar. (**b**) Experimentally obtained Ar-induced pressure broadening of the NO absorption lines fitted with a linear model. The residual between the data and the fit is displayed below.

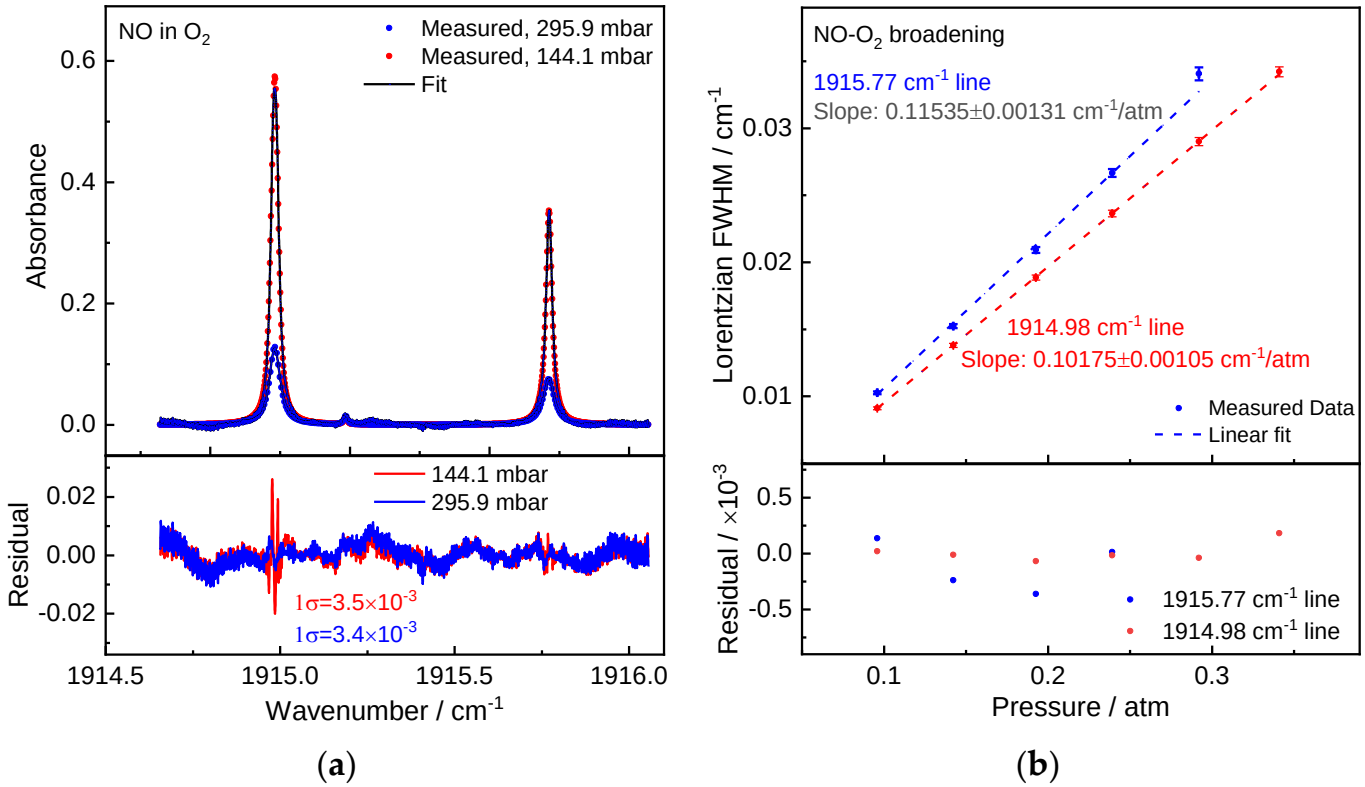


Figure 5. (**a**) Measured NO absorption spectra (20-scan average) in O_2 at pressures 144.1 mbar and 295.9 mbar. Below is a display of the residual between the measured and fitted values. (**b**) Obtained NO P(5) (1←0) pressure broadening absorption line caused by O_2 and fitted with a linear model. Below is a display of the fit-to-data residual.

4.5. Broadening Coefficient, He

Figure 6a shows the measured NO absorption spectrum at pressures of 929.1 mbar and 294.3 mbar. The corresponding Lorentzian widths exhibit excellent pressure linearity. The experiments yielded the NO-He broadening coefficients γ_{He} = 44.17(23) × 10^{-3} cm^{-1}/atm and 37.79(22) × 10^{-3} cm^{-1}/atm for Peak 1 and Peak 2, respectively.

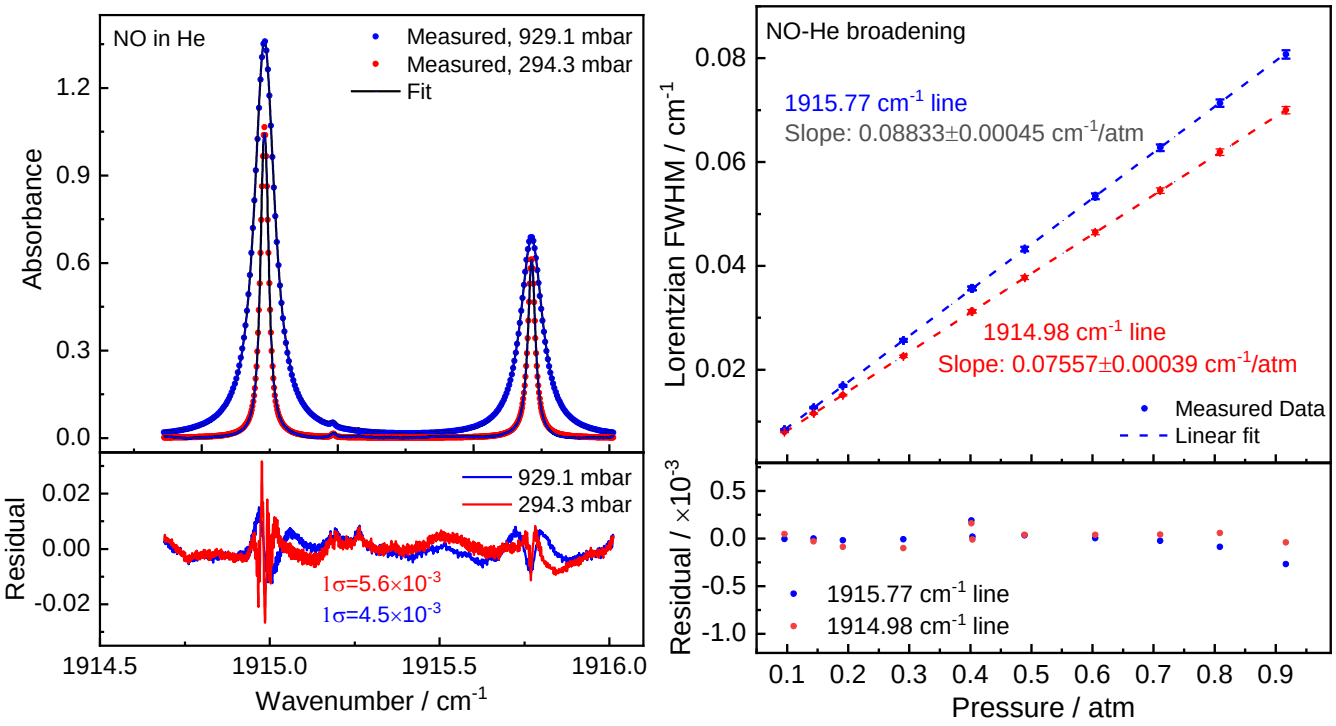


Figure 6. (**a**) Measured NO absorption spectra (20-scan average) in He at pressures of 929.1 mbar and 294.3 mbar. Below is a comparison of the residual between measured and fitted data, which results in an SNR of about 200. (**b**) Measured He-induced pressure broadening of the NO absorption lines fitted with a linear model. Below is a display of the residual between fit and data.

4.6. Broadening Coefficient, H_2

Pure H_2 was utilized as the buffer gas in this measurement of the NO-H2 broadening coefficient (purity 5.0, Linde). Figure 7a provides an illustration of a measured NO in O_2 absorption spectra at total pressures of 167.9 mbar and 671.4 mbar. The Voigt profile was used to fit the NO in the H_2 spectrum after it had been averaged over 20 scans. The optical density (spectral fitting residuals) was close to (1σ) 3 × 10^{-3}. According to the slope of the linear regression of the Lorentzian widths vs. pressures, the measured NO-H_2 broadening coefficients for Peaks 1 and 2 are γ_{H2} = 71.67(43) ×10^{-3} cm^{-1}/atm and 62.77(38) × 10^{-3} cm^{-1}/atm.

4.7. Literature Comparison

Table 2 summarizes our results at 294 K, along with the literature values of the NO (1←0) R11.5 (Ω3/2 and Ω1/2) lines from various published papers [20,28–31]. Note that we did not convert the broadening coefficients to the same temperature (at 300 K) as those in the literature for this comparison. The tabulated broadening coefficients are also shown in Figure 8. The different buffer gas means a different atom/molecule, and a different molecule has different collision frequency, energy and efficiency, which lead to different collision effects, and therefore, different broadening behavior. From the measurement results, the Ar broadening coefficient is the smallest, and the largest is the CO_2 broadening coefficient. For

$NO\text{-}CO_2$ and $NO\text{-}H_2$ broadening coefficients, there are no available reference data to compare. To the best of our knowledge, these two coefficients have not been reported before.

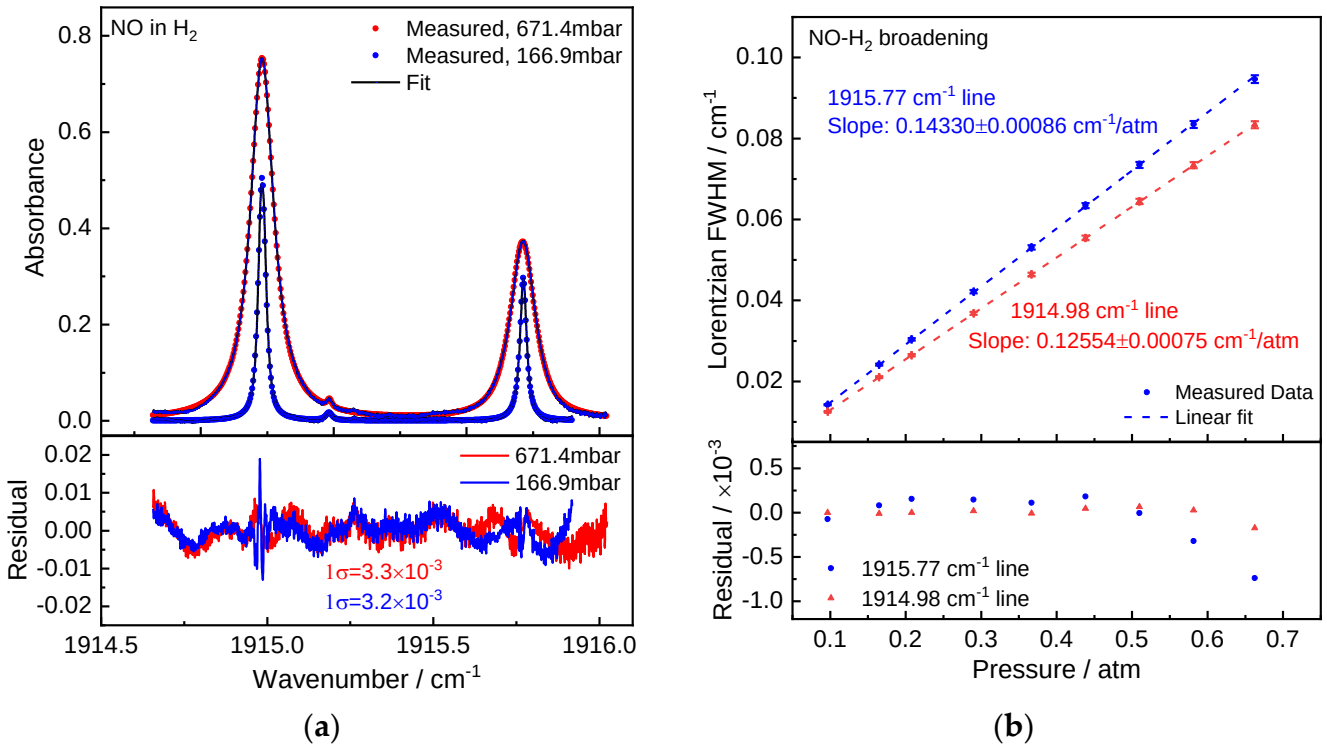


Figure 7. (**a**) Measured NO absorption spectra (20-scan averaged) in H_2 at pressures of 671.4 mbar and 166.9 mbar. Below is a comparison of the residual between measured and fitted data, which results in an SNR of over 200. (**b**) Measured H_2-induced pressure broadening of the NO absorption lines fitted linearly. Below is a display of the fit-to-data residual.

Table 2. Comparison of our findings with information from the literature regarding the NO (1←0) R (11.5) absorption lines' broadening coefficients when combined with N_2, CO_2, Ar, H_2, O_2, He, and Air.

	R11.5 Ω3/2	**R11.5 Ω1/2**
γ_{CO2} [10^3 cm^{-1}/atm]	79.99 ± 0.44	72.92 ± 0.52
Pressure range [atm]	0.1–0.7	0.1–0.7
Relative error [%]	0.55%	0.71%
γ_{N2} [10^3 cm^{-1}/atm]	58.13 ± 0.31	50.8 ± 0.27
Pressure range [atm]	0.1–0.9	0.1–0.9
Relative error [%]	0.53%	0.53%
Ref. [28]	57.16(40)	54.57(54)
Ref. [29]	61.4(8)	58.1(9)
γ_{Ar} [10^3 cm^{-1}/atm]	42.64 ± 0.22	37.67 ± 0.19
Pressure range [atm]	0.1–1.0	0.1–1.0
Relative error [%]	0.52%	0.50%
Ref. [20]	47.88(1.5)	49.4(1.5)
γ_{O2} [10^3 cm^{-1}/atm]	57.68 ± 0.66	50.88 ± 0.53
Pressure range [atm]	0.1–0.3	0.1–0.4
Relative error [%]	1.14%	1.04%
Ref. [30]	49.00(30)	47.50(67)
γ_{H2} [10^3 cm^{-1}/atm]	71.67 ± 0.43	62.77 ± 0.38
Pressure range [atm]	0.1–0.7	0.1– 0.7
Relative error [%]	0.60%	0.61%

Table 2. *Cont.*

	R11.5 Ω3/2	R11.5 Ω1/2
γ_{He} [10^3 cm^{-1}/atm]	44.17 ± 0.23	37.79 ± 0.20
Pressure range [atm]	0.1–1.0	0.1–1.0
Relative error [%]	0.52%	0.53%
Ref. [20]	51.86(0.76)	48.64(1.5)
γ_{Air} [10^3 cm^{-1}/atm]	58.04 ± 0.71	50.82 ± 0.63
Pressure range [atm]	0.1–0.9	0.1–0.9
Relative error [%]	1.23%	1.23%
Ref. [31]	59	
Ref. [25]	56.1(2.8)	53.7(2.7)

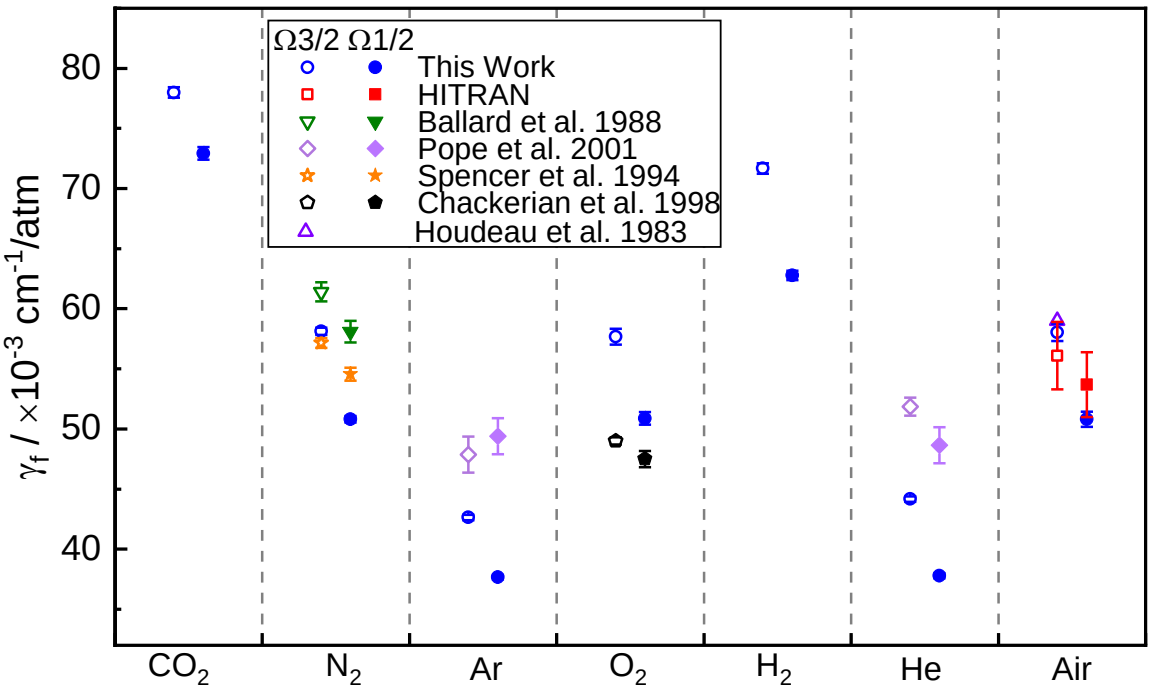


Figure 8. Comparison of our findings to published data from the literature. Solid points: R11.5 Ω3/2, Open points: R11.5 Ω1/2 [20,28–31].

N_2:O_2 = 79:21 is used to determine the NO-air broadening coefficient in Table 2 based on the measured NO-N_2 and NO-O_2 broadening coefficients. Peaks 1 and 2 have computed NO-Air broadening coefficients of 58.04(71) × 10^{-3} cm^{-1}/atm and 50.82(63) × 10^{-3} cm^{-1}/atm, respectively, at 294 K. Within the measurement uncertainty, the NO-air broadening coefficient determined by our study and based on our measured NO-O_2 and NO-N_2 values agrees well with HITRAN and Ref. [31].

The relative difference to [30] for the O_2-induced pressure broadening coefficient is 15% for R11.5 Ω3/2 and 6.7% for R11.5 Ω1/2, while the measured temperatures in this reference were 299 K, 5 K higher than our result. The measured NO-N_2 broadening coefficient shows a better agreement with the literature value in Ref. [28] than the value in Ref. [29].

There are significant deviations of about 10 to 20% for NO-Ar and NO-He broadening coefficients compared to the measured results in Ref. [20]. This is due to the temperature difference. The broadening coefficients reported in Ref. [20] are for 300 K. Moreover, in this work as well as in the literature [20], the broadening coefficients of R11.5 Ω3/2 lines should be larger than R11.5 Ω1/2. However, in Ref. [20], the reported R11.5 NO-Ar broadening coefficients are the opposite.

5. Conclusions

We report the pressure broadening coefficients of the NO R(11.5) Ω3/2 and Ω1/2 lines in the 1←0 bands at 1915.77 cm^{-1} and 1914.98 cm^{-1} caused by N_2, CO_2, Ar, H_2, O_2, He and Air, measured using a Mid-IR ICL-based TDLAS spectrometer. The NO-CO_2, NO-N_2, NO-Ar, NO-O_2, NO-H_2 and NO-He pressure broadening coefficients were measured for the pressure range of 100–970 mbar at 294 K using high-quality gases. The measured NO-N_2 and NO-O_2 data were used to compute the NO-Air broadening coefficients. Using the MID-IR TDLAS spectrometer, including both hardware and software, as well as the calibrated pressure and temperature sensors (SI traceable), the experimental findings provide accurate and repeatable results utilizing the same equipment and evaluation procedure. We analyzed the newly measured results to existing data from the literature and addressed the discrepancy. When compared to published data, the relative precision of the measured pressure broadening coefficients show significant improvement. For the first time, the newly measured NO-CO_2 and NO-H_2 broadening coefficients were reported. The obtained broadening coefficients in this work have been used for quantifying the NO amount fraction in a recent publication of a gas-phase study of ammonia in a shock tube reactor which employed a fixed wavelength TDLAS spectrometer. The broadening coefficients can also be used in all industrial and energy gas applications, especially for monitoring the combustion process as well as the NO emission quantification.

Author Contributions: Conceptualization, S.A. and Z.Q.; methodology, S.A. and Z.Q.; formal analysis, S.A. and Z.Q.; writing—original draft preparation, S.A. and D.Z.; writing—review and editing, all authors. All authors have read and agreed to the published version of the manuscript.

Funding: We (Denghao Zhu and Sumit Agarwal) would like to acknowledge the Alexander von Humboldt (AvH) Foundation for financial support. The State of Lower Saxony/Germany's funding within the H2-WaVe project Grant number ZN3772 is gratefully acknowledged.

Institutional Review Board Statement: Not applicable.

Informed Consent Statement: Not applicable.

Data Availability Statement: Not applicable.

Conflicts of Interest: The authors declare no conflict of interest.

References

1. Lu, X.; Ye, X.; Zhou, M.; Zhao, Y.; Weng, H.; Kong, H.; Li, K.; Gao, M.; Zheng, B.; Lin, J.; et al. The Underappreciated Role of Agricultural Soil Nitrogen Oxide Emissions in Ozone Pollution Regulation in North China. *Nat. Commun.* **2021**, *12*, 5021. [CrossRef] [PubMed]
2. Logan, J.A. Nitrogen oxides in the troposphere: Global and regional budgets. *J. Geophys. Res. Atmos.* **1983**, *88*, 10785–10807. [CrossRef]
3. Price, C.; Penner, J.; Prather, M. NO_x from lightning: 1. Global distribution based on lightning physics. *J. Geophys. Res. Atmos.* **1997**, *102*, 5929–5941. [CrossRef]
4. Ravishankara, A.R.; Daniel, J.S.; Portmann, R.W. Nitrous oxide (N_2O): The dominant ozone-depleting substance emitted in the 21st century. *Science* **2009**, *326*, 123–125. [CrossRef] [PubMed]
5. Yienger, J.J.; Levy, H. Empirical model of global soil-biogenic NOχ emissions. *J. Geophys. Res. Atmos.* **1995**, *100*, 11447–11464. [CrossRef]
6. Steinfeld, J.K. Atmospheric chemistry and physics: From air pollution to climate change. *Environ. Sci. Policy Sustain. Dev.* **1998**, *40*, 26. [CrossRef]
7. Delmas, R.; Serça, D.; Jambert, C. Global inventory of NOx sources. *Nutr. Cycl. Agroecosys.* **1997**, *48*, 51–60. [CrossRef]
8. Aithal, S.M. Modeling of NOx Formation in Diesel Engines Using Finite-Rate Chemical Kinetics. *Appl. Energy* **2010**, *87*, 2256–2265. [CrossRef]
9. Miller, J.A.; Bowman, C.T. Mechanism and Modeling of Nitrogen Chemistry in Combustion. *Prog. Energy Combust. Sci.* **1989**, *15*, 287–338. [CrossRef]
10. Menzel, L.; Kosterev, A.; Curl, R.; Tittel, F.; Gmachl, C.; Capasso, F.; Sivco, D.; Baillargeon, J.; Hutchinson, A.; Cho, A.; et al. Spectroscopic detection of biological NO with a quantum cascade laser. *Appl. Phys. B Laser Opt.* **2001**, *72*, 859–863. [CrossRef]
11. Almodovar, C.A.; Spearrin, R.M.; Hanson, R.K. Two-Color Laser Absorption near 5 Mm for Temperature and Nitric Oxide Sensing in High-Temperature Gases. *J. Quant. Spectrosc. Radiat. Transf.* **2017**, *203*, 572–581. [CrossRef]

12. Chao, X.; Jeffries, J.B.; Hanson, R.K. Wavelength-Modulation-Spectroscopy for Real-Time, in Situ absorption sensor for NO in Combustion Gases with a 5.2 μm Quantum-Cascade Laser. *Proc. Comb. Inst.* **2011**, *33*, 725–733. [CrossRef]
13. Qu, Z.; Schmidt, F.M. In Situ H2O and Temperature Detection Close to Burning Biomass Pellets Using Calibration-Free Wavelength Modulation Spectroscopy. *Appl. Phys. B* **2015**, *119*, 45–53. [CrossRef]
14. Qu, Z.; Ghorbani, R.; Valiev, D.; Schmidt, F.M. Calibration-Free Scanned Wavelength Modulation Spectroscopy—Application to H_2O and Temperature Sensing in Flames. *Opt. Express* **2015**, *23*, 16492. [CrossRef] [PubMed]
15. Qu, Z.; Steinvall, E.; Ghorbani, R.; Schmidt, F.M. Tunable Diode Laser Atomic Absorption Spectroscopy for Detection of Potassium under Optically Thick Conditions. *Anal. Chem.* **2016**, *88*, 3754–3760. [CrossRef]
16. Liu, Y.; Lin, J.; Guo, Y. Measurement of the Pressure-Broadening Coefficient of NO by Saturation Spectroscopy of LMR. *Can. J. Phys.* **2000**, *78*, 989–995. [CrossRef]
17. Lundqvist, S.; Margolis, J.; Reid, J. Measurements of Pressure-Broadening Coefficients of NO and O_3 Using a Computerized Tunable Diode Laser Spectrometer. *Appl. Opt.* **1982**, *21*, 3109. [CrossRef]
18. Spencer, M.N.; Chackerian, C.; Giver, L.P.; Brown, L.R. Temperature Dependence of Nitrogen Broadening of the NO Fundamental Vibrational Band. *J. Mol. Spectrosc.* **1997**, *181*, 307–315. [CrossRef]
19. Pine, A.S.; Maki, A.G.; Chou, N.Y. Pressure Broadening, Lineshapes, and Intensity Measurements in the 2 ← 0 Band of NO. *J. Mol. Spectrosc.* **1985**, *114*, 132–147. [CrossRef]
20. Pope, R.S.; Wolf, P.J. Rare Gas Pressure Broadening of the NO Fundamental Vibrational Band. *J. Mol. Spectrosc.* **2001**, *208*, 153–160. [CrossRef]
21. Vyrodov, A.O.; Heinze, J.; Meier, U.E. Collisional Broadening of Spectral Lines in the A-X System of NO. *J. Quant. Spectrosc. Radiat. Transf.* **1995**, *53*, 277–287. [CrossRef]
22. Chang, A.Y.; DiRosa, M.D.; Hanson, R.K. Temperature Dependence of Collision Broadening and Shift in the NO A ← X (0, 0) Band in the Presence of Argon and Nitrogen. *J. Quant. Spectrosc. Radiat. Transf.* **1992**, *47*, 375–390. [CrossRef]
23. Qu, Z.; Nwaboh, J.A.; Li, G.; Werhahn, O.; Ebert, V. Measurements of N_2, CO_2, Ar, O_2 and Air Pressure Broadening Coefficients of the HCL p(5) Line in the 1–0 Band Using an Interband Cascade Laser. *Appl. Sci.* **2021**, *11*, 5190. [CrossRef]
24. Qu, Z.; Werhahn, O.; Ebert, V. Thermal Boundary Layer Effects on Line-of-Sight Tunable Diode Laser Absorption Spectroscopy (TDLAS) Gas Concentration Measurements. *Appl. Spectrosc.* **2018**, *72*, 853–862. [CrossRef] [PubMed]
25. Gordon, I.E.; Rothman, L.S.; Hargreaves, R.J.; Hashemi, R.; Karlovets, E.V.; Skinner, F.M.; Conway, E.K.; Hill, C.; Kochanov, R.V.; Tan, Y.; et al. The HITRAN2020 Molecular Spectroscopic Database. *J. Quant. Spectrosc. Radiat. Transf.* **2022**, *277*, 107949. [CrossRef]
26. Qu, Z.; Nwaboh, J.; Werhahn, O.; Ebert, V. Towards a DTDLAS-Based Spectrometer for Absolute HCl Measurements in Combustion Flue Gases and a Better Evaluation of Thermal Boundary Layer Effects. *Flow. Turbul. Combust.* **2021**, *106*, 533–546. [CrossRef]
27. Zhu, D.; Qu, Z.; Li, M.; Agarwal, S.; Fernandes, R.; Shu, B. Investigation on the NO formation of ammonia oxidation in a shock tube applying tunable diode laser absorption spectroscopy. *Combust. Flame* **2022**, *246*, 112389. [CrossRef]
28. Spencer, M.N.; Chackerian, C.; Giver, L.P.; Brown, L.R. The Nitric Oxide Fundamental Band: Frequency and Shape Parameters for Rovibrational Lines. *J. Mol. Spectrosc.* **1994**, *165*, 506–524. [CrossRef]
29. Ballard, J.; Johnston, W.B.; Kerridge, B.J.; Remedios, J.J. Experimental Spectral Line Parameters in the 1-0 Band of Nitric Oxide. *J. Mol. Spectrosc.* **1988**, *127*, 70–82. [CrossRef]
30. Chackerian, C.; Freedman, R.S.; Giver, L.P.; Brown, L.R. The NO Vibrational Fundamental Band: O2-Broadening Coefficients. *J. Mol. Spectrosc.* **1998**, *192*, 215–219. [CrossRef]
31. Houdeau, J.P.; Boulet, C.; Bonamy, J.; Khayar, A.; Guelachvili, G. Air Broadened NO Linewidths in a Temperature Range of Atmospheric Interest. *J. Chem. Phys.* **1983**, *79*, 1634–1640. [CrossRef]

Disclaimer/Publisher's Note: The statements, opinions and data contained in all publications are solely those of the individual author(s) and contributor(s) and not of MDPI and/or the editor(s). MDPI and/or the editor(s) disclaim responsibility for any injury to people or property resulting from any ideas, methods, instructions or products referred to in the content.